Solar-Terrestrial Physics. 2026, vol. 12, iss.1, pp. 105–113. DOI: 10.12737/stp-121202612. © 2026
N.M. Gavrilov, S.P. Kshevetski, A.V. Koval, Yu.A. Kurdyaeva. Published by INFRA-M Academic Publishing House

DOI: 10.12737/stp-121202612
EDN: IDYRNC

Received July 19, 2025
Accepted October 16, 2025

CRITICAL LEVEL INFLUENCE ON SPECTRA OF SECONDARY GRAVITY WAVES IN THE MIDDLE AND UPPER ATMOSPHERE

N.M. Gavrilov
St. Petersburg State University,
Saint Petersburg, Russia, n.gavrilov@spbu.ru

S.P. Kshevetski
St. Petersburg State University,
Saint Petersburg, Russia, renger@mail.ru
I. Kant Baltic Federal University,
Kaliningrad, Russia

A.V. Koval
St. Petersburg State University,
Saint Petersburg, Russia, a.v.koval@spbu.ru

Yu.A. Kurdyaeva
West Department of Pushkov Institute of Terrestrial Magnetism, Ionosphere and Radio Wave Propagation RAS,
Kaliningrad, Russia, yakurdyaeva@gmail.com

Abstract. A high-resolution nonlinear numerical model is used to simulate propagation of internal gravity waves (IGWs) from the troposphere to the upper atmosphere. This simulation takes into account background wind profiles containing critical levels at which the horizontal wind velocity becomes equal to the horizontal phase speed of IGW. According to traditional linear theories of atmospheric waves, near critical levels the vertical wavelength approaches zero, which should lead to a strong dissipation of IGWs propagating from the troposphere and may significantly decrease their amplitudes in the upper atmosphere. The wave sources in the model are defined as vertical velocity perturbations propagating along the Earth surface. The mean horizontal wind in the atmosphere is approximated by the Gaussian profile with a maximum at an altitude of 50 km. We analyze the spectra of wave fields near critical levels and at a distance from them. It has been found that the instability of waves near critical levels intensifies the energy transition from primary IGWs propagating from surface sources to secondary wave modes. This causes an increase in spectral peaks at wavelengths shorter than the horizontal length of primary IGW. Therefore, above critical levels, spectral modes with shorter horizontal wavelengths begin to prevail with increasing altitude, and the amplitudes of these secondary waves at the same altitudes can exceed the amplitudes of analogous primary IGW propagating in the absence of critical levels in the middle atmosphere.

Keywords: acoustic-gravity waves, spectrum, secondary waves, numerical simulation, upper atmosphere, middle atmosphere.

INTRODUCTION

Internal gravity waves (IGWs) are an important component of the dynamics of the middle and upper atmosphere. These waves play an important role in solar-terrestrial physics, connecting phenomena in the lower and upper atmosphere, as well as influencing Earth's ionosphere. A significant part of IGWs is generated in the lower atmosphere, in particular due to the space-time irregularity of atmospheric heating because of absorption of solar radiation. Then IGWs propagate to high altitudes with an increase in the amplitude of disturbances due to a decrease in atmospheric density. This results in the formation of wave-like ionospheric irregularities affecting geophysical fields and radio wave propagation.

Waves generated in the lower atmosphere transfer energy and momentum to the mesosphere and thermosphere. Due to dissipation and transfer of momentum to the mean flow, IGWs can lead to significant variations in hydrodynamic parameters of the atmosphere, up to a reversal of zonal circulation in the mesosphere and lower thermosphere (MLT), and affect the circulation in the middle and upper atmosphere, including the thermosphere and the ionosphere [Yiğit, Medvedev, 2009; Miyoshi et al., 2014]. Therefore, for more detailed study of the atmosphere dynamics, space weather, and solar-terrestrial relationships, progress is needed in understanding the processes associated with IGWs.

To account for IGW effects in the general atmospheric circulation model, parameterizations of mesoscale waves and their influence on the mean flow are used which should be compared with observations [Alexander et al., 2010]. There are numerical models of global circulation on a fine spatiotemporal mesh [Becker, Vadas, 2018], but resolution of these models makes it possible to describe only IGWs with long horizontal lengths. In this regard, when developing climate models and integrated models of atmospheric and ionospheric circulation, effective schemes for parameterizing dynamic and thermal IGW effects are still needed.

Recently, the numerical simulation of nonlinear IGW and turbulence in the atmosphere has been actively developing. In [Bidlingmeier, Pogoreltsev, 1992; Pogoreltsev, Pertsev, 1995], numerical simulation of IGWs propagating upward from the troposphere and triggering ionospheric disturbances was carried out. The works [Fritts et al., 2009, 2014] are devoted to simulation of disruption of IGWs accompanied by formation of Kelvin—Helmholtz instability in atmospheric regions with small vertical and horizontal dimensions. Numerical 2D

models of IGW in the atmosphere were used in [Yu et al., 2009; Liu et al., 2008].

Gavrilov and Kshevetskii [2014] developed a numerical 3D model with high space-time resolution, which describes the behavior of nonlinear IGWs in the atmosphere from the Earth surface to the thermosphere. The algorithm of the model takes correctly into account the laws of conservation of energy, momentum, mass and the thermodynamic law of nondecreasing entropy [Gassmann, Herzog, 2015]. This model can find physically based generalized solutions of hydrodynamical equations, and the computational scheme is stable in the regions of instability of nonlinear waves and turbulence generation, where many numerical algorithms become unstable. Such a stable algorithm makes the numerical model [Gavrilov, Kshevetskii, 2014] applicable to study IGWs and their disruption in a wide range of altitudes, facilitating closer examination of the mechanisms of dynamic interactions between different atmospheric layers.

Propagation of nonlinear IGWs in the middle and upper atmosphere is accompanied by cascade energy transfer across the spectrum to smaller-scale wave modes [Gavrilov et al., 2022; Gavrilov, Kshevetskii, 2023]. Lengths and periods of such secondary modes of the first type are shorter than primary nonlinear IGWs generated by wave sources in the atmosphere. Secondary IGWs of the first type can accelerate the transition of wave energy to turbulence.

Moreover, disruption of primary IGWs can lead to spatial irregularities of wave accelerations and heat inflows on scales that are comparable to horizontal dimensions of wave packets [Vadas et al., 2003, 2018]. Such irregularities, in turn, can create secondary wave modes of the second type, whose lengths and periods are longer than those of primary IGWs. Secondary waves of both the first and second types may have horizontal phase velocities and vertical lengths greater than those of primary IGWs [Vadas, Liu, 2013; Vadas et al., 2023]. Such fast IGWs are less susceptible to dissipation due to their molecular and turbulent viscosity and thermal conductivity. They can reach higher altitudes and transfer momentum and energy more efficiently to the thermosphere [Vadas et al., 2023].

Occurrence and evolution of secondary IGW modes today seem to be an important and poorly understood process that can significantly affect the mechanisms of wave momentum and energy transformation and transfer. For example, of particular interest are regions of convective and dynamic instability in which amplitudes of primary IGWs can considerably increase and the generation of secondary wave modes can be greatly intensified.

More detailed study of secondary IGWs is facilitated by the application of numerical models with high space-time resolution and by the development of methods for separating spectra of primary and secondary IGW modes. Gavrilov et al. [2025] illustrate the possibility of generating secondary waves near critical levels at which the horizontal wave phase velocity is equal to the mean wind velocity, which causes instability and disruption of IGWs.

Gavrilov and Kshevetskii [2023] developed a method that makes it possible to separate horizontal spatial spectra obtained by the 3D nonlinear high-resolution model, which are created by primary and secondary IGWs at different altitudes in the atmosphere at fixed instants of time. It was shown that some time after activation of a wave source on the Earth surface peaks of secondary waves with large horizontal wave numbers, multiples of the wave numbers of primary IGW, appear in the spectra. This separation of primary and secondary IGW spectra allows us to estimate relative amplitudes of secondary wave modes at different times, at different altitudes, and with different stability of average wind and atmospheric temperature profiles.

In this paper, the method developed by Gavrilov and Kshevetskii [2023] is used to separate and then analyze in detail the evolution of spectra of primary and secondary IGWs if there are critical levels, studied in [Gavrilov et al., 2025], in the vertical profile of the background wind. Near critical levels, the vertical length of primary IGW decreases significantly and the wave becomes unstable, which makes it possible to expect a more intense amplification of spectral components other than the primary wave [Bowman et al., 1980]. This separation method can demonstrate differences between spectra of secondary atmospheric IGWs for the presence and absence of critical levels in the background wind profile.

1. NUMERICAL MODEL

In this paper, we employ a numerical three-dimensional model with high space-time resolution to describe nonlinear IGWs in the atmosphere [Gavrilov, Kshevetskii, 2014]. The model uses complete three-dimensional hydrodynamic equations in the plane geometry approximation [Gavrilov, Kshevetskii, 2014]. It includes nonlinear processes and dissipation, which affect the IGW behavior in the atmosphere, and enables us to study such complex processes as instability and disruption of IGW, as well as turbulence generation.

The average temperature profiles $T_0(z)$ for the calculations are taken from the semi-empirical atmospheric model NRLMSISE-00 [Picone et al., 2002]. Mean coefficients of molecular thermal conductivity and viscosity are calculated by the Sutherland formula [Kikoin, 1976]. This model also takes into account background turbulent thermal conductivity and viscosity whose coefficients are maximum (to 10 m^2/s) in the surface layer and in the lower thermosphere and minimum (to 0.1 m^2/s) in the stratosphere (see [Gavrilov, Kshevetskii, 2014]).

Zero values of vertical velocity and vertical gradients of horizontal velocity and temperature are used at the upper boundary [Gavrilov, Kshevetskii, 2014]. These boundary conditions cause reflection of IGWs coming from the lower layer of atmosphere. In this study, the upper boundary is set at an altitude of 600 km, at which the molecular thermal conductivity and viscosity are very high, and waves reflected from the upper boundary fade rapidly. Testing shows that at distances of more than two heights of the homogeneous atmosphere from the upper boundary the influence of upper boundary conditions can be ignored, so at altitudes up to 200 km, considered in this paper, the influence of upper boundary conditions is negligible. At the

lower boundary (on the Earth surface), the boundary conditions are written as follows (see [Gavrilov, Kshevetskii, 2014]):

$$\begin{aligned} &(T')_{z=0} = 0,\ (u)_{z=0} = 0,\ (v)_{z=0} = 0, \\ &(w)_{z=0} = W_0 \cos\left(\sigma t - \vec{k}_h \cdot \vec{r}\right), \end{aligned} \quad (1)$$

where T', w, u, v are wave variations of temperature and velocity components along the vertical z-axis and the horizontal x and y axes respectively. In (1), the expression for the vertical velocity at the lower boundary is utilized as a source of plane IGWs in the model. Here, σ and W_0 are the observed frequency and amplitude of an excited primary wave; $\vec{r}(x, y)$ and $\vec{k}_h(k_x, k_y)$ are the horizontal radius vector and wave vector, where k_x and k_y are horizontal wave numbers along the x and y axes respectively. In this study, the horizontal x-axis is directed parallel to the horizontal wave vector; therefore, for primary IGW $k_h=k_x$ and $k_y=0$.

Monochromatic wave components (1) can be interpreted as components of Fourier transform of turbulent, convective, and mesometeorological processes. Such processes can be approximated by superposition of effective spectral components of vertical velocity on the Earth surface [Townsend, 1965, 1966].

Numerical calculations begin under windless atmospheric conditions with stationary profiles of average density, temperature, molecular viscosity, and molecular weight according to the NRLMSISE-00 model [Picone et al., 2002] for 50° N in January at moderate solar activity (F10.7=150 s.f.u.). The temperature profile used in the simulation is shown in the top panel of Figure 1.

To analyze the influence of critical levels on the IGW behavior, the projection of the stratomesospheric jet stream on the direction of the primary wave is approximated by a Gaussian function with a maximum of 80 m/s at an altitude of 50 km (bottom panel in Figure 1). This wind profile coincides with the wind model adopted in [Gavrilov et al., 2025].

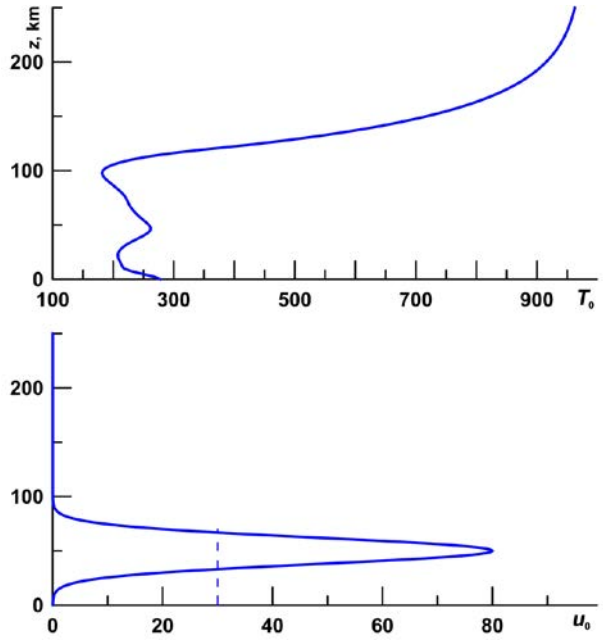

Figure 1. Vertical profile of the mean zonal background temperature [K] for January at 50° N (top) and model Gaussian profile of the projection of wind speed on the direction of the horizontal wave vector [m/s] (bottom). The dashed line indicates the horizontal phase IGW velocity used in the calculations

Previous experiments with this model have demonstrated that sudden activation of wave source (1) can form a great initial wave momentum that can reach the upper atmosphere in a few minutes. To ensure smooth activation of the wave source, in the described simulation the amplitude W_0 in (1) is multiplied by a Gaussian function, which increases from zero at t=0 to 1 at $t=t_a$ (see details in [Gavrilov et al., 2022]). In this study, t_a is considered as the time of activation of the wave source in the model, and at $t>t_a$ the amplitude of the source W_0 in (1) is constant.

It is natural to assume that for small W_0 in (1) the numerical solution for the lower atmosphere at $t \gg t_a$ should aim for stable waves described by the linear theory of atmospheric IGWs (e.g., [Gossard, Hooke, 1975]). Gavrilov et al. [2015] demonstrated that simulated amplitude ratios of different wave fields correlate well with the polarization ratios of the linear IGW theory [Gossard, Hooke, 1975] for $t \gg t_a$ at 100 km.

In this paper, we analyze primary IGWs generated by ground source (1), which propagate parallel to the x-axis. The horizontal size of the analyzed atmospheric region L_h=800 km. Periodic conditions are used at the boundaries of this horizontal region (see [Gavrilov, Kshevetskii, 2014]). In the simulation, we employed wave source (1) with k_y=0 and an IGW amplitude W_0=0.01–0.1 mm/s. Low amplitudes correspond to weak IGWs when nonlinear effects are negligible. Source (1) at W_0~0.1 mm/s produces intense IGWs and significant nonlinear interactions in the upper atmosphere [Gavrilov, Kshevetskii, 2023].

The number of horizontal lengths of primary wave within the analyzed region n=4, which corresponds to the horizontal length of wave $\lambda_h=L_h/n$=200 km and acoustic-gravity wave (AGW) periods $\tau=\lambda_h/c_h$~1.9–0.6 hr for the range of horizontal phase velocity values c_h~30–100 m/s. The step of the horizontal grid of the numerical model $\Delta x=\lambda_h/32$, and the time step is selected automatically and amounts to several seconds. The vertical grid of the model covers altitudes from the Earth surface to 600 km and contains 1024 unequally spaced nodes. The vertical grid step varies from 12 m in the surface layer to 3 km near the upper boundary; hence almost 70 % of the grid nodes are located in the troposphere and middle atmosphere.

Section 3 presents the simulation results for c_h=30 m/s intrinsic to IGWs with a relatively long vertical length, which can propagate from the Earth surface to the upper atmosphere.

2. IDENTIFICATION OF SPECTRUM OF SECONDARY AGWs

Similarly to [Gavrilov, Kshevetskii, 2023], spectra of simulated wave fields versus the horizontal wavenumber are calculated at different instants of time for horizontal

planes located at fixed altitudes. The calculated variable f_i is set on the horizontal grid with coordinates x_i(i=1, 2, ..., N) on the given plane. To identify Fourier transform components for each $k_h \approx k_x$, the set of f_i values is approximated by the sum

$$f_c = X(k_h)\cos(k_h x) + Y(k_h)\sin(k_h x). \quad (2)$$

After using the least square method to determine the cosine and sine Fourier transforms $X(k_h)$ and $Y(k_h)$, the amplitude $A_f(k_h)$ and the spectral density $S_f(k_h)$ can be found from formulas

$$A_f(k_h) = \sqrt{X^2 + Y^2},\ S_f(k_h) = \frac{L_h A_f^2}{2\pi}. \quad (3)$$

Applying (2) and (3) is equivalent to the popular Lomb—Scargle spectral analysis method [Lomb, 1976; Scargle, 1982]. If grid nodes x_i are equidistant, (2) and (3) yield a result equivalent, say, to the fast Fourier transform. Approximation (2) by the least square method is also possible for unequally spaced grid nodes. Figure 2 of [Gavrilov, Kshevetskii, 2023] shows the spectral density $S_w(k_h)$ of vertical velocity at various altitudes.

The use of wave source (1) and the excitation of plane primary IGW with horizontally uniform amplitude distribution at the lower boundary allow us to separate the spectra of primary and secondary waves, which have horizontal lengths different from the horizontal length of the primary wave. Horizontal velocity inhomogeneities in the numerical model can cause local variations in the horizontal wavenumber of primary IGW k_{h1}. Because of this, the spectral maximum associated with primary IGW can widen and occupy a narrow range of wavenumbers $k_h \in [k_{h1} - \varepsilon, k_{h1} + \varepsilon]$ near the main maximum at $k_h = k_{h\,1}$. The spectral density of secondary IGWs $S'_f(k_h)$ can therefore be obtained by excluding all spectral components that fall within the ε-neighborhood of k_h. The spectrum $S'_f(k_h)$ in $k_h \in [k_{h1} - \varepsilon, k_{h1} + \varepsilon]$ can be replaced by linear interpolation between spectral density values at the boundaries of the interval. An example of identification of the spectrum of secondary IGWs is given in Figure 1 in [Gavrilov, Kshevetskii, 2023]. The said separation of spectra makes it possible to find variances of perturbations of the function f: δ^2_{f1} and δ^2_{f2}, which are caused by primary and secondary IGW modes respectively:

$$\delta^2_{f1} = \int_{k_{h1-\varepsilon}}^{k_{h1+\varepsilon}} S_f(k_h)\,dk_h,$$
$$\delta^2_{f2} = \int_{k_{h0}}^{k_{hm}} S'_f(k_h)\,dk_h, \quad (4)$$

where k_{h0} and k_{hm} are minimum and maximum boundaries of the spectral region under study.

3. SIMULATION RESULTS

The purpose of this work is to examine the effect of critical levels on propagation of primary IGW and the formation of the spectrum of secondary wave modes. We make calculations for IGW source (1) with a horizontal phase velocity c_h=30 m/s. Such IGW has a vertical length of ~10 km and can propagate without significant attenuation to ~100 km.

If a wave propagates eastward in the direction of the mean flow in the winter middle atmosphere, it can reach a critical level at which $c_h = u_0$. In the bottom panel in Figure 1, there are two critical levels corresponding to

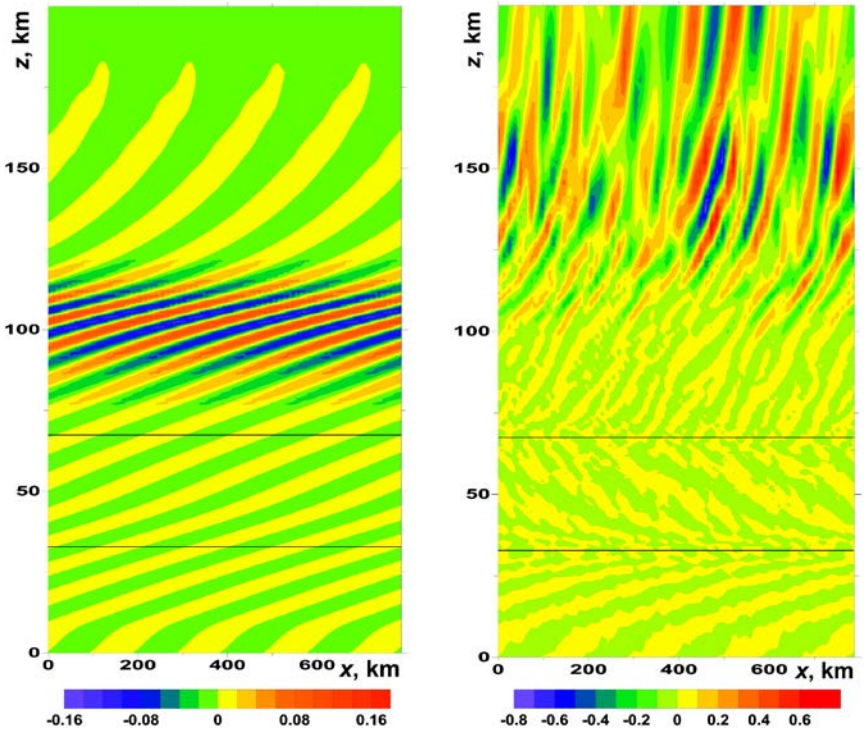

Figure 2. Model wave fields of vertical velocity [m/s] in the XOZ plane in a windless atmosphere (left) and in the presence of critical levels in the mean wind profile (right) for IGW with c_h=30 m/s and wave source amplitude (1) W_0=0.1 mm/s at t=52 hr after the start of the simulation. Horizontal lines indicate heights of critical levels

intersections of the mean wind profile and the dashed line indicating c_h=30 m/s. Heights of these critical levels in Figure 1 are ~33 and 67 km.

The left panel in Figure 2 shows the cross-section of simulated vertical velocity wave field by a vertical plane passing through the horizontal *x*-axis in a windless atmosphere with the vertical temperature profile from Figure 1 for *t*=52 hr after activation of wave source (1) at the lower boundary and stabilization of wave oscillations at the altitudes of interest. There are constant phase surfaces inclined to the horizon below 100 km and characteristic of atmospheric IGWs. According to the theory of plane linear stationary IGWs in a windless atmosphere (e.g., [Gossard, Hooke, 1975]), the angle of wavefront inclination to the horizon is $\arcsin(\tau_b/\tau)$, where τ_b and τ are the Brunt—Väisälä and IGW periods. This corresponds to the theoretical vertical wavelength $\lambda_z \approx c_h \tau_b$ that yields λ_z~9–12 km for c_h=30 m/s at $\tau_b \sim (3–4)\cdot 10^2$ s peculiar to the temperature profile at altitudes 50–100 km in January in Figure 1. Estimates of the distance between successive inclined wavefronts in the left panel in Figure 2 give $\lambda_z \approx 10$ km at 50–100 km, which matches the above range of theoretical λ_z values.

In the right panel of Figure 2 is the vertical velocity field similar to that shown in the left panel, but for the mean wind profile from Figure 1, which is prescribed at the initial time. Horizontal lines at ~33 and 67 km in Figure 2 denote two critical levels (see the bottom panel in Figure 1), where the mean wind velocity is equal to the horizontal wave phase velocity.

The right panel in Figure 2 indicates that between the two critical levels the direction of inclination of wavefronts to the *x*-axis is reversed. This is due to the fact that the primary IGW intrinsic frequency $\omega=\sigma-k_x u_0$ becomes negative between the critical levels. Upward IGWs have a positive vertical component of wave energy flux $\overline{p'w'} \sim -\rho_0 \omega U^2/(2m) > 0$, where ρ and *p* are density and pressure; *m* and *U* are vertical wavenumber and amplitude of horizontal velocity variations; strokes and overline mark wave variations and wave period averaging respectively. Maintaining positive $\overline{p'w'}$ during ω sign reversal corresponds to *m* sign reversal and a change in the direction of inclination of the wavefronts to the horizon between the lower and upper critical levels in the right panel of Figure 2.

Comparing the left and right panels in Figure 2 shows that the wave field penetrates above critical levels, although the linear IGW theory predicts that the energy of a plane primary wave should undergo strong dissipation near a critical level and decrease significantly when passing it [Bowman et al., 1980]. However, in the right panel, IGW amplitudes at altitudes above 120 km in the presence of critical levels are much higher than those of primary IGW for a windless atmosphere in the left panel. This can occur, in particular, as a result of transfer of primary IGW energy to other wave modes due to convective instability of the temperature and wind wave profile in the vicinity of the critical level and propagation of these secondary modes above the critical level [Bowman et al., 1980].

Furthermore, in the right panel above 100 km the wave field has 2–3 times as many maxima and minima along the *x*-axis as in the left panel for primary IGW, which has four maxima and minima. The same result was obtained in [Gavrilov et al., 2025]. This testifies that secondary waves are generated which may have horizontal lengths shorter than primary IGW and which may prevail in the upper atmosphere above critical levels. Simulation of IGW spectra by the nonlinear model [Gavrilov, Kshevetskii, 2023] has revealed that the secondary wave modes with horizontal lengths 2–3 times shorter than those of primary IGW have maximum amplitudes.

Figure 3 presents model horizontal spatial spectra of IGWs in the troposphere and stratosphere. In left panels in Figure 3 (for a windless atmosphere and in the absence of critical levels), the maximum corresponding to horizontal wave number of primary IGW k_{h1} predominates. In the right panels of Figure 3 in the presence of a critical level in the mean wind profile, the primary IGW amplitude at 10 km is approximately the same as in the windless atmosphere. Near and above critical levels at 30 km and 50 km, the spectral density of primary IGW in the right panels is much lower than that in the windless atmosphere in the left panels. At the same time, the spectral density of secondary waves with $k_h > k_{h1}$ near and above the critical level is 1–2 orders of magnitude higher in the right panels than in the left ones.

Figure 4 displays spectra similar to those in Figure 3 for MLT heights. The maximum corresponding to primary IGW with $k_h=k_{h1}$ is seen to prevail, and the spectral density of secondary waves with $k_h>k_{h1}$ in the windless atmosphere

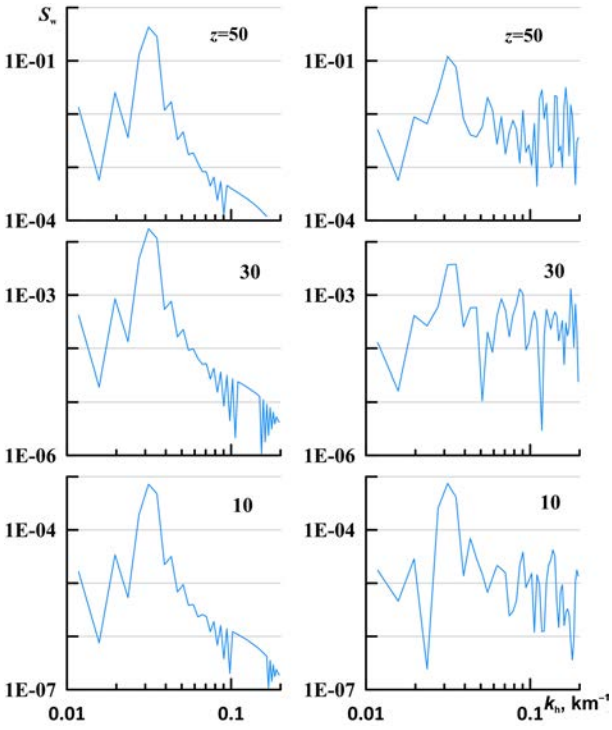

Figure 3. Spectral density of vertical velocity wave field $S_w(k_h)$ [m^3 s^{-2}] in a windless atmosphere (left) and in the presence of critical levels in the mean wind profile (right) for IGW with c_h=30 m/s and wave source amplitude (1) W_0=0.1 mm/s at *t*=52 hr at different altitudes (marked with numbers in km)

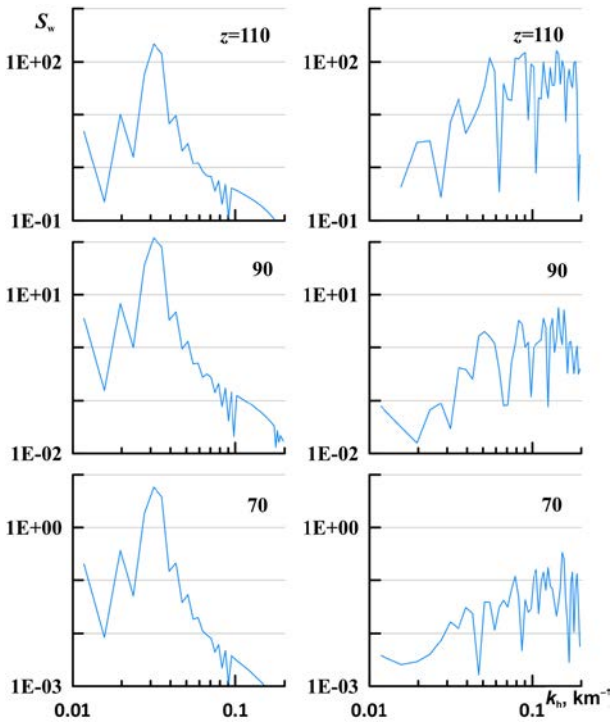

Figure 4. The same as in Figure 3, but for the altitude range 70–110 km

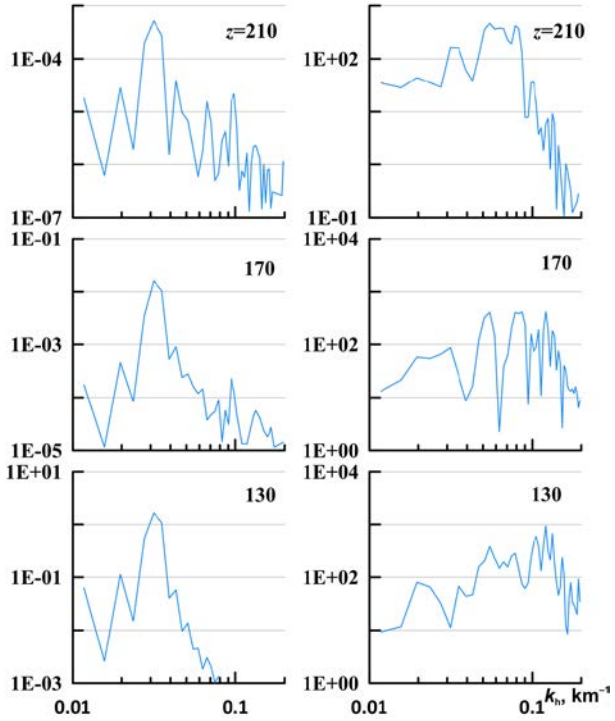

Figure 5. The same as in Figure 3, but for the altitude range 130–210 km

is low (left panels). At 70 km near and above the upper critical level, the maximum intrinsic to primary IGW is practically absent in the right panels, and secondary waves predominate in the spectra. Spectral densities in Figure 4 increase with height due to a decrease in atmospheric density, since dissipation of relatively long IGWs is low.

Figure 5 illustrates spectra similar to those presented in Figures 3 and 4, but for different levels in the thermosphere. In the left panels in Figure 5, as in Figures 3 and 4, the maxima typical of primary IGW with $k_h=k_{h1}$ dominate, yet the corresponding spectral densities are several orders of magnitude lower than those above critical levels in the right panels. This is due to strong dissipation of primary IGW under the action of high molecular viscosity and thermal conductivity in the thermosphere. Some of the secondary wave modes generated near critical levels in the middle atmosphere can have high horizontal phase velocities and long vertical lengths and can propagate to high altitudes in the atmosphere.

Right panels in Figure 5 suggest that as the altitude increases, enhancement of dissipation leads to a decrease in spectral density at large wave numbers. Therefore, the spectrum in the right panels becomes narrower and is limited to small wave numbers. Interestingly, at 210 km a maximum appears at $k_h=k_{h1}$, similar to the primary wave, in the right panel, but its spectral density is almost six orders of magnitude higher than that of primary IGW in the corresponding left panel. This suggests that the wave mode with $k_h=k_{h1}$ at 210 km has c_h and λ_h larger than for primary IGW. Such a fast wave can occur as a result of nonlinear interactions in the spectrum of secondary IGWs. This assumption is confirmed by the results obtained in [Zhao et al., 2017], where an increase in vertical wavelengths with height was experimentally shown, which is attributed to generation of long secondary IGWs by shorter waves dominating in the stratosphere.

Table lists model RMS values (standard deviations) of vertical velocity variations, caused by primary IGW and secondary wave modes, at different altitudes for a windless atmosphere and in the presence of critical levels. Variance of disturbances generated by primary and secondary IGWs was estimated according to Formula (4) after separating spectra of primary and secondary IGWs, as described in Section 2. The amplitude of the primary wave (proportional to δ_{w10}) in a windless atmosphere is seen to increase to an altitude of 100 km, and then it decreases under the effect of high molecular viscosity and thermal conductivity so that primary IGW practically disappears above 150 km. The relative contribution of secondary waves to vertical velocity pulsations in a windless atmosphere is small and varies little with height.

In the presence of critical levels, the amplitude of primary IGW in Table increases in the troposphere and stratosphere at altitudes below the first critical level in Figure 1 and is approximately equal to the amplitude of the primary wave in a windless atmosphere. A sharp retardation in the growth rate of δ_{w1} as compared to δ_{w10} near critical levels at 30 and 70 km (see Table) occurs due to dissipation of wave energy and its transition to secondary wave modes. At 70–80 km, δ_{w1} values are only 5 % of the corresponding δ_{w10} values. At the same time, amplitudes of secondary waves increase significantly in the vicinity of critical levels so that at 70–90 km δ_{w2} is 9–11 times higher than δ_{w1}. In the upper atmosphere, δ_{w2} prevails up to ~200 km.

Table shows an increase in δ_{w1} (amplitude of IGW with $k_h=k_{h1}$) at all altitudes from 70 km to 250 km so that at 250 km $\delta_{w1}>\delta_{w2}$. However, this wave cannot be the primary IGW generated by wave source (1), since even in

Altitude dependence of the model [mm/s] RMS variations in vertical velocity, which are generated by primary IGW (δ_{w10}, δ_{w1}) and secondary wave modes (δ_{w20}, δ_{w2}), as well as their ratios. The "zero" index indicates the values obtained for a windless atmosphere.

z, km	Windless atmosphere			With critical levels			Ratios	
	δ_{w10}	δ_{w20}	$\delta_{w20}/\delta_{w10}$	δ_{w1}	δ_{w2}	δ_{w2}/δ_{w1}	δ_{w1}/δ_{w10}	δ_{w2}/δ_{w20}
0	0.07	0.02	0.22	0.07	0.02	0.23	0.99	1.00
10	0.11	0.02	0.22	0.11	0.07	0.62	1.02	2.87
20	0.22	0.05	0.22	0.23	0.13	0.58	1.06	2.81
30	0.53	0.12	0.22	0.26	0.36	1.36	0.46	3.08
40	1.22	0.26	0.22	0.59	0.83	1.41	0.50	3.13
50	2.62	0.58	0.22	1.36	1.88	1.38	0.53	3.26
60	4.90	1.10	0.22	0.98	2.57	2.61	0.20	2.34
70	9.57	2.14	0.22	0.61	5.22	8.59	0.05	2.44
80	20.1	4.45	0.22	1.12	12.3	11.0	0.05	2.77
90	43.6	9.69	0.22	2.47	22.8	9.25	0.06	2.35
100	83.4	18.7	0.22	8.63	63.3	7.34	0.10	3.38
110	58.5	12.7	0.22	16.4	135.1	8.23	0.30	10.6
130	5.15	1.15	0.22	36.3	250.8	6.91	64.8	217.7
150	1.43	0.31	0.22	33.4	312.9	9.38	16.5	1007.3
170	0.50	0.12	0.25	39.4	194.6	4.94	73.9	1563.2
190	0.23	0.07	0.29	40.8	199.4	4.89	161.1	3024.5
210	0.09	0.03	0.39	56.3	168.2	2.99	558.5	4868.8
250	0.08	0.03	0.42	82.6	67.3	0.81	1006.0	2098.1

a windless atmosphere δ_{w10} for primary IGW is insignificant above 150 km, and in the presence of critical levels the primary wave is practically absorbed below 70 km (see Table). The reason for large δ_{w1} may be the reverse transition of the energy of secondary waves to IGW with $k_h = k_{h1}$, which, nonetheless, has a horizontal phase velocity and a vertical length greater than the primary wave. Such IGW dissipates less under the effect of molecular viscosity and thermal conductivity and can propagate to high altitudes in the atmosphere.

In [Zhao et al., 2017; Becker and Vadas, 2018], IGWs in the middle atmosphere were studied using lidar observations of temperature variations. It was found that vertical lengths and horizontal phase velocities of IGWs at altitudes 30–40 km are usually less than the simultaneously observed ones in the mesosphere and lower thermosphere.

Becker and Vadas [2018] adopt a high-resolution general circulation model, which allows direct modeling of IGW with relatively large horizontal (λ_h>165 km) and vertical (λ_z>1.5 km) wavelengths. The authors show that secondary IGWs with large λ_z can be generated at altitudes slightly above the maximum velocity of the polar vortex. Comparison of the simulation results with lidar measurements has revealed that λ_z is smaller in the stratosphere and larger in the mesosphere due to the generation of long secondary wave modes.

Vadas et al. [2023] studied IGW propagation through a polar vortex in the stratosphere and found that upward and downward secondary wave modes are generated at 50–60 km, where primary IGWs dissipate and create inhomogeneous wave accelerations and heat inflows generating long secondary waves of the second type. The upward and downward secondary waves were observed with a Rayleigh lidar at the Alomar Observatory in northern Norway and were simulated by the general circulation model HIAMCM, which has sufficient resolution to identify long IGWs. In the context of our calculations using the high-resolution model, the generation of downward secondary waves near critical levels can explain the increased values of δ_{w2} in Table at 10–20 km, which exceed the corresponding values of δ_{w20} for a windless atmosphere.

IGW simulation at altitudes from the Earth surface to the thermosphere is carried out in [Vadas et al., 2024]. The authors show that IGWs generated below and inside the polar vortex dissipate and produce inhomogeneous wave accelerations and heat inflows in the upper stratosphere and lower mesosphere, which excite secondary wave modes. Secondary waves increase with height, become unstable, collapse, and generate waves of the next order. This process is repeated and can give rise to mesoscale and large-scale high-order wave modes in the thermosphere. These waves can have vertical lengths much longer than primary IGWs in the lower atmosphere. The simulation results agree well with satellite, lidar, and meteor radar observations. Thus, jet streams in the middle atmosphere can lead to the generation of high-order wave modes with long vertical lengths in the thermosphere through multi-stage

interaction between nonlinear waves as they propagate vertically.

The simulation carried out in this work confirms the importance of secondary IGW modes for the dynamics of the middle and upper atmosphere. Increased generation of secondary waves near critical levels of jet streams in the middle atmosphere can enhance IGW activity in the thermosphere. The results of analysis of only the secondary wave spectra as a function of the horizontal wavenumber are presented above. It can be expected that the frequency spectra of secondary waves are no less wide and cover significant frequency ranges. The spectrum of secondary waves can therefore contain components with large horizontal phase velocities that correspond to long vertical wavelengths. This allows us to explain the results of our simulation, namely that the spectrum of secondary waves generated by primary IGW in the middle atmosphere may hold components that are characterized by lower dissipation and can create significant wave disturbances in the thermosphere. Critical levels of the vertical profile of the background velocity in the middle atmosphere can enhance the generation of secondary wave modes. The upward components of these secondary modes with long vertical lengths can cause disturbances in the upper atmosphere that are more intense than the direct effect of primary IGW propagating in a windless atmosphere.

This paper presents results for only one value of the amplitude, horizontal wavelength, and phase velocity of the wave source at the lower boundary of the atmosphere, as well as one vertical temperature profile and one vertical structure of the atmospheric jet stream. Changes in these parameters can affect the conditions of energy and momentum exchange between primary IGW, background flow, and secondary waves. Further research is required to study the dependence of characteristics of secondary wave modes coming into the thermosphere from surface wave sources on the model parameters listed above.

CONCLUSION

In this paper, we have simulated atmospheric IGWs, using the nonlinear model with high space-time resolution. The algorithm was applied which allows us to separate the spectrum of primary IGWs excited by a wave source on the Earth surface and the spectrum of secondary waves generated by primary waves at different heights of the atmosphere. The simulation takes into account background wind profiles containing critical levels at which the horizontal wind velocity becomes equal to the horizontal phase velocity of IGW.

According to the traditional linear theory of atmospheric waves, the vertical wavelength approaches zero near critical levels, which should lead to a strong dissipation of IGWs propagating from the troposphere and a significant decrease in their amplitudes in the upper atmosphere. The model wave sources are defined as vertical velocity perturbations propagating along the Earth surface. The jet stream in the atmosphere is approximated by the Gaussian profile of the mean zonal wind with a maximum at 50 km.

The simulation carried out in this work confirms the importance of secondary IGW modes for the dynamics of the middle and upper atmosphere. Critical levels of the vertical profile of the background velocity in the middle atmosphere can enhance the generation of secondary wave modes. The instability of waves near critical levels intensifies the energy transition from the background flow and primary IGWs from surface sources to secondary wave modes. This leads to an increase in spectral peaks at wavelengths shorter than the horizontal length of primary IGW.

Increased generation of secondary waves near critical levels in the middle atmosphere can enhance IGW activity in the thermosphere. Our simulation shows that the spectrum of secondary waves generated by primary IGW in the middle atmosphere, despite shorter horizontal wavelengths, may contain components with longer vertical wavelengths, which have less dissipativity and can create significant wave disturbances in the thermosphere. Upward components of these secondary modes with long vertical lengths can cause disturbances in the upper atmosphere that are more intense than the direct effect of primary IGW propagating in a windless atmosphere.

The dependence of characteristics of secondary IGWs excited near critical levels on the parameters of primary IGWs and changes in background temperature and wind profiles call for further investigation.

This research was financially supported by the Russian Science Foundation (Grant No. 25-17-00166).

REFERENCES

Alexander M.J., Geller M., McLandress C., et al. Recent developments in gravity-wave effects in climate models and the global distribution of gravity-wave momentum flux from observations and models. *Quarterly J. Royal Meteorological Society. Part A.* 2010, vol. 136, pp. 1103–1124. DOI: 10.1002/qj.637.

Becker E., Vadas S.L. Secondary gravity waves in the winter mesosphere: Results from a high-resolution global circulation model. *J. Geophys. Res. Atmos*. 2018, vol. 23, iss. 5, pp. 2605–2627. DOI: 10.1002/2017JD027460.

Bidlingmeier E.R., Pogoreltsev A.I. Numerical modeling of the transformation of acoustic-gravity waves into temperature and viscous waves in the atmosphere. *Izvestia. Atmospheric and Oceanic Physics*. 1992, vol. 28, iss. 1, pp. 64–74. (In Russian).

Bowman M.R., Thomas I., Thomas R.H. The propagation of gravity waves through a critical layer for conditions of moderate wind shear. *Planetary and Space Sci.* 1980, vol. 28, iss. 2, pp. 119–133.DOI: 10.1016/0032-0633(80)90088-4.

Fritts D.C., Wang L., Werne J. Gravity wave-fine structure interactions: A reservoir of small-scale and large-scale turbulence energy. *Geophys. Res. Lett*. 2009, vol. 36, iss. 19, L19805. DOI: 10.1029/2009GL039501.

Fritts D.C., Wan K., Werne J., et al. Modeling the implications of Kelvin—Helmholtz instability dynamics for airglow observations. *J. Geophys. Res. Atmos*. 2014, vol. 119, pp. 8858–8871. DOI: 10.1002/2014JD021737.

Gassmann A., Herzog H.-J. How is local material entropy production represented in a numerical model? *Quarterly J. Royal Meteorological Society*. 2015, vol. 141, pp. 854–869. DOI: 10.1002/qj.2404.

Gavrilov N.M., Kshevetskii S.P. Identification of spectrum of secondary acoustic-gravity waves in the middle and upper atmosphere in a high-resolution numerical model. *Sol.-Terr. Phys.* 2023, vol. 9, iss. 3, pp. 86–92. DOI: 10.12737/stp-93202310.

Gavrilov N.M., Kshevetskii S.P. Numerical modeling of the propagation of nonlinear acoustic-gravity waves in the middle and upper atmosphere. *Izvestiya, Atmos. Oceanic Phys*. 2014, vol. 50, iss. 1, pp. 66–72. DOI: 10.7868/S0002351513050040.

Gavrilov N.M., Kshevetskii S.P., Koval A.V. Verifications of the high-resolution numerical model and polarization relations of atmospheric acoustic-gravity waves. *Geoscientific Model Development*. 2015, vol. 8, pp. 1831–1838. DOI: 10.5194/gmd-8-1831-2015

Gavrilov N.M., Kshevetskii S.P., Koval A.V. Decay times of atmospheric acoustic-gravity waves after deactivation of wave forcing. *Atmos. Chem. Phys*. 2022, vol. 22, pp. 3713–3724. DOI: 10.5194/acp-22-13713-2022.

Gavrilov N.M., Kshevetskii S.P., Koval A.V., Kurdyaeva Yu.A. Tunneling of acoustic-gravity waves through critical levels to the upper atmosphere. *Adv. Space Res*. 2025, vol. 75, iss. 4, pp. 3661–3670. DOI: 10.1016/j.asr.2024.12.005.

Gossard E.E., Hooke W.H. *Waves in the Atmosphere: Atmospheric Infrasound and Gravity Waves: Their Generation and Propagation*. Elsevier Sci. Publ. Co., 1975, 456 p.

Kikoin I.K. *Tables of Physical Quantities*. Moscow, Atomizdat Publ., 1976, pp. 272–279. (In Russian).

Liu X., Xu J., Liu H., Ma R. Nonlinear interactions between gravity waves with different wavelengths and diurnal tide. *J. Geophys. Res.: Atmos*. 2008, vol. 1139, iss. 8, D08112. DOI: 10.1029/2007JD009136.

Lomb N. Least-squares frequency analysis of unequally spaced data. *Astrophys. Space Sci*. 1976, vol. 39, iss. 2, pp. 447–462.

Miyoshi Y., Fujiwara H., Jin H., Shinagawa H. A global view of gravity waves in the thermosphere simulated by a general circulation model. *J. Geophys. Res. Space Phys*. 2014, vol. 119, iss. 7, pp. 5807–5820. DOI: 10.1002/2014JA019848.

Picone J.M., Hedin A.E., Drob D.P., Aikin A.C. NRLMSISE-00 empirical model of the atmosphere: Statistical comparisons and scientific issues. *J. Geophys. Res*. 2002, vol. 107, iss. A12, 1468. DOI: 10.1029/2002JA009430.

Pogoreltsev A.I., Pertsev N.N. The influence of background wind on the formation of acoustic-gravity waves structure in the thermosphere. *Izvestia. Atmospheric and Oceanic Physics*, 1996, vol. 31, iss. 6, pp. 723–728.

Scargle J.D. Studies in astronomical time series analysis. II – Statistical aspects of spectral analysis of unevenly spaced data. *Astrophys. J.* 1982, vol. 263, pp. 835–853. DOI: 10.1086/160554.

Townsend A.A. Excitation of internal waves by a turbulent boundary layer. *J. Fluid Mechanics*. 1965, vol. 22, pp. 241–252. DOI: 10.1017/S002211206500071X.

Townsend A.A. Internal waves produced by a convective layer. *J. Fluid Mechanics*. 1966, vol. 24, pp. 307–319. DOI: 10.1017/S0022112066000661.

Vadas S.L., Liu H.-L. Numerical modeling of the large-scale neutral and plasma responses to the body forces created by the dissipation of gravity waves from 6 h of deep convection in Brazil. *J. Geophys. Res.: Space Phys*. 2013, vol. 118, pp. 2593–2617. DOI: 10.1002/jgra.50249.

Vadas S.L., Fritts D.C., Alexander M.J. Mechanism for the generation of secondary waves in wave breaking regions. *J. Atmos. Sci*. 2003, vol. 60, iss. 1, pp. 194–214. DOI: 10.1029/2004JD005574.

Vadas S.L., Zhao J., Chu X., Becker E. The excitation of secondary gravity waves from local body forces: Theory and observation. *J. Geophys. Res.: Atmos*. 2018, vol. 123, iss. 17, pp. 9296–9325. DOI: 10.1029/2017JD027970.

Vadas S.L., Becker E., Bossert K., et al. Secondary gravity waves from the stratospheric polar vortex over ALOMAR Observatory on 12–14 January 2016. *J. Geophys. Res.: Atmos*. 2023, vol 128, e2022JD036985. DOI: 10.1029/2022JD036985.

Vadas S.L., Becker E., Bossert K., et al. The role of the polar vortex jet for secondary and higher-order gravity waves in the northern mesosphere and thermosphere during 11–14 January 2016. *J. Geophys. Res.: Space Phys*. 2024, vol. 129, iss. 9, e2024JA032521. DOI: 10.1029/2024JA032521.

Yiğit E., Medvedev A.S. Heating and cooling of the thermosphere by internal gravity waves. *Geophys. Res. Lett*. 2009, vol. 36, L14807. DOI: 10.1029/2009GL038507.

Yu Y., Hickey M.P., Liu Y. A numerical model characterising internal gravity wave propagation into the upper atmosphere. *Adv. Space Res*. 2009, vol. 44, pp. 836–846. DOI: 10.1016/j.asr.2009.05.014.

Zhao J., Chu X., Chen C., et al. Lidar observations of stratospheric gravity waves from 2011 to 2015 at McMurdo (77.84° S, 166.69° E), Antarctica: 1. Vertical wavelengths, periods, and frequency and vertical wave number spectra. *J. Geophys. Res.: Atmos*. 2017, vol. 122, iss. 10, pp. 5041–5062. DOI: 10.1002/2016JD026368.

Original Russian version: Gavrilov N.M., Kshevetski S.P., Koval A.V., Kurdyaeva Yu.A., published in Solnechno-zemnaya fizika. 2026, vol. 12, no. 1, pp. 115–124. DOI: 10.12737/szf-121202612.

How to cite this article

Gavrilov N.M., Kshevetski S.P., Koval A.V., Kurdyaeva Yu.A. Critical level influence on spectra of secondary gravity waves in the middle and upper atmosphere. *Sol.-Terr. Phys.* 2026, vol. 12, iss. 1, pp. 105–113. DOI: 10.12737/stp-121202612.